Limits on spacetime foam

Wayne A. Christiansen and Y. Jack Ng

Department of Physics and Astronomy, University of North Carolina, Chapel Hill, North Carolina 27599, USA

David J. E. Floyd

School of Physics, University of Melbourne, Melbourne, Victoria 3010, Australia

Eric S. Perlman

Physics and Space Sciences Department, Florida Institute of Technology, Melbourne, Florida 32901, USA

Plausibly spacetime is foamy on small distance scales, due to quantum fluctuations. We elaborate on the proposal to detect spacetime foam by looking for seeing disks in the images of distant quasars and active galactic nuclei. This is a null test in the sense that the continued presence of unresolved point sources at the milliarcsecond level in samples of distant compact sources puts severe constraints on theories of quantized spacetime foam at the Planckian level. We discuss the geometry of foamy spacetime, and the appropriate distance measure for calculating the expected angular broadening. We then deal with recent data and the constraints they put on spacetime foam models. While time lags from distant pulsed sources such as gamma ray bursts have been posited as a possible test of spacetime foam models, we demonstrate that the time-lag effect is rather smaller than has been calculated, due to the equal probability of positive and negative fluctuations in the speed of light inherent in such models. Thus far, images of high-redshift quasars from the Hubble ultra-deep field provide the most stringent test of spacetime foam theories. While random-walk models ($\alpha = 1/2$) have already been ruled out, the holographic ($\alpha = 2/3$) model remains viable. Here $\alpha \sim 1$ parametrizes the different spacetime foam models according to which the fluctuation of a distance l is given by $\sim l^{1-\alpha} l_P^\alpha$ with l_P being the Planck length. Indeed, we see a slight wavelength-dependent blurring in the ultra-deep field images selected for this study. Using existing data in the *Hubble Space Telescope* (HST) archive we find it is impossible to rule out the $\alpha = 2/3$ model, but exclude all models with $\alpha < 0.65$. By comparison, current gamma ray burst time-lag observations only exclude models with $\alpha < 0.3$.

I. INTRODUCTION

Even at the minute scales of distance and duration examined with increasingly discriminating instruments, spacetime still appears to be smooth and structureless. But, like everything else, (plausibly) spacetime is subject to quantum fluctuations. So we expect that spacetime, probed at a small enough scale, will appear complicated—something akin in complexity to a turbulent froth that [1] has dubbed "quantum foam," also known as "spacetime foam." But how large are the fluctuations in the fabric of spacetime? How small a scale is small enough so that the foaminess of spacetime manifests itself? To quantify the problem, let us recall that, if spacetime indeed undergoes quantum fluctuations, there will be an intrinsic limitation to the accuracy with which one can measure a macroscopic distance, for that distance fluctuates. Denoting the fluctuation of a distance l by δl, on general grounds, we expect $\delta l \gtrsim N l^{1-\alpha} l_P^\alpha$, [2] where N is a numerical factor ~ 1 and $l_P = \sqrt{\hbar G/c^3}$ is the Planck length, the characteristic length scale in quantum gravity, and we have denoted the Planck constant, gravitational constant and the speed of light by $\hbar$, G and c respectively. It is important to note that δl cannot be defined without reference to the macroscopic distance, l (i.e., δl is not defined locally). The parameter $\alpha \lesssim 1$ specifies the different spacetime foam models. We note that smaller values of α necessarily lead to larger distance fluctuations and, hence, such models are easier to test observationally.

Because the Planck length ($\sim 10^{-33}$ cm) is so incredibly small, we need an astronomically large distance l for its fluctuation δl to be detectable. Even so, measurement of δl is not trivial. It must be calibrated against a known length standard. The most obvious calibrator is the wavelength λ, of the light received from a distant source. Thus, in principle, distance fluctuations $\pm \delta l$, imply phase fluctuations $\pm \Delta \phi = \pm 2\pi \delta l/\lambda$ (c.f. [3–5]). More recently, Christiansen *et al.* [6], henceforth CNvD, suggested that fluctuations in the direction of the local wave-vector, $\pm \delta \psi \equiv \pm \Delta \phi/(2\pi) = \pm \delta l/\lambda$, could possibly be detected as "halos" in images of distant "point sources". However, it must be noted that using the wavelength of received light to bootstrap a calibration for measuring δl necessarily involves interferometry and/or wave optics such as Strehl analysis (see Sec. IV). The point is that, due to quantum foam-induced fluctuations in the phase

velocity of an incoming light wave from a distant point source, the wave front itself develops a small scale "cloud of uncertainty" equivalent to a foamy structure. This results in the wave vector, upon detection, acquiring a jitter in direction with an angular spread of the order of $\delta\psi$. In effect, spacetime foam creates a "seeing disk" whose angular diameter is

$$\delta\psi = N\left(\frac{l}{\lambda}\right)^{1-\alpha}\left(\frac{l_P}{\lambda}\right)^{\alpha}. \quad (1)$$

For a telescope or interferometer with baseline length D, this means that dispersion (on the order of $\delta\psi$ in the normal to the wave front) will be recorded as a spread in the angular size of a distant point source, causing a reduction in the Strehl ratio and/or the fringe visibility when $\delta\psi \sim \lambda/D$ for a diffraction-limited telescope. Thus, in principle, for arbitrarily large distances spacetime foam sets a lower limit on the observable angular size of a source at a given wavelength λ. Furthermore, the disappearance of "point sources" will be strongly wavelength-dependent happening first at short wavelengths. In fact, as we show below, the frequency dependence of blurring currently offers the best chance to detect the effects of spacetime foam.

As discussed by CNvD, there are three major theoretical models for specifying the cumulative effects of spacetime foam:

(i) The random-walk model [7] in which the spacetime foam effects grow like a one-dimensional random-walk, corresponding to $\alpha = 1/2$, $N = 1$.

(ii) The holographic model [8–10] which is consistent with the holographic principle [11,12] where the information content in any three-dimensional region of space can be encoded on a two-dimensional surface surrounding the region of interest, corresponding to $\alpha = 2/3$ and $0.97 \leq N \leq 1.9$ as discussed in Sec. II.

(iii) An anticorrelation model [13] in which there are no cumulative effects, so the distance fluctuation remains simply the Planck length, corresponding to $\alpha = 1$, $N = 1$.

The random-walk model can be ruled out on the basis of HST observations of relatively nearby quasars (distance $\sim$1 Gpc) according to CNvD. The predicted spacetime foam-induced seeing disks ($\sim$ few $\times 10^{-4}$ radians) clearly exceed the HST resolution even in the IR waveband at 800 nm (3.3×10^{-7} radians). Although the holographic model's seeing disk ($\sim 10^{-8}$ radians) is still an order of magnitude smaller than the nominal IR HST resolution, at larger distances (redshifts $z \gtrsim 1$) and shorter wavelengths HST may have sufficient resolution to test this model also. On the other hand, the anticorrelation model with $\delta\psi \sim l_P/\lambda$ will likely remain untestable by astronomical means since the effect is vanishingly small and independent of distance.

Testing models of spacetime foam requires large distances to maximize the effect which, therefore, requires

that cosmological effects must be taken into account. The fundamental cosmological distance measure is the *comoving distance* (c.f. [14]). However, other distance measures may be used, depending on circumstances. For example, the *luminosity distance* is commonly used to interpret observations of high-redshift objects (as used, for example, by [15], in his study of spacetime foam angular broadening). However, luminosity distance is inappropriate for studying spacetime foam-induced angular broadening. The reason is that the luminosity distance has a built-in energy dependence because it is based on the flux detected by a distant observer. Therefore, the redshift dependence of the luminosity distance explicitly includes a correction for the diminished energy received from distant sources. That enhances the expected angular broadening (c.f. Eq. (1)). However, the angular broadening caused by spacetime foam does not explicitly depend on flux. Another distance measure, the angular diameter distance, may be appropriate for observations involving lensing or scattering. However, spacetime foam angular uncertainties are not associated with scattering or lensing (see Sec. IV for detailed discussion). Quantum foam is, by definition, a property of the fabric of spacetime itself, and not an extrinsic property measured against the background geometry. Therefore the appropriate cosmological distance measure is the fundamental *comoving distance*, which we shall use in our subsequent calculations.

In addition, other factors also make the search for observable effects more complicated for the following reasons:

(1) Sensitivity: More distant sources are fainter. This means that, as far as interferometry is concerned, the lack of observed fringes may simply be due to the lack of sufficient flux rather than the possibility that the instrument has resolved a spacetime foam-generated halo. This is probably the most serious limitation on experiments to search for spacetime foam. As discussed above, the effect is cumulative, requiring large distances to appear. But large distances inevitably mean faint sources.

(2) Atmospheric turbulence: Integration times must be shorter than atmospheric fluctuation times. Thus, again what one needs is to find a bright but sufficiently distant external source, for then the integration times may be short enough to allow one to remove or at least minimize the atmospheric effects. Of course, the latter problem does not intrude for space-based observatories such as HST or *Chandra*, nor for an interferometer.

(3) Masking: This may originate under two distinct circumstances:

(a) The source may have an intrinsic structure comparable in angular size to the expected spacetime foam halo;

(b) Any competing scattering mechanism in the intervening medium between source and observer (e.g., gravitational wave scattering of light, micro-lensing by machos or dark matter, etc.)

Concerning (a), distant sources may have extended structures. Thus, if fringes are not seen, it may be an indication that the source quasar has an intrinsic core structure whose angular size is comparable to, or larger than, the spacetime foam halo. Since we do not know the physical scales of all components of AGN and quasars we may find that spacetime foam effects are masked by intrinsic structures. However, since the angular size of intrinsic structures decreases like l^{-1} (in a flat universe) whereas spacetime foam halos *increase* as $l^{1-\alpha}$, statistical samples can, in principle, separate the two effects.

The bottom line is that a number of modern telescopes including the Very Large Telescopes in interferometric mode (VLTI), HST and *Chandra* are on the verge of testing theories of spacetime foam (see, e.g., [15]), providing a sufficiently large sample of sufficiently bright compact sources can be developed. This is where future large aperture telescopes will prove to be crucial. The test is simply a question of the detection of a reduction in Strehl ratio or correspondingly a reduction in interferometer fringe amplitude. It is not a question of mapping the structure of the predicted seeing disk. Knowing the real sensitivity limits of the telescopes involved will enable us to search the catalogs to see if we can find some quasars that exceed the sensitivity limits.

One of the purposes of this paper is to give a more quantitative analysis of the proposal just described. For that, the order of magnitude estimate for δl available so far is not enough. In the next section, we will calculate the numerical factor in the δl expression.

A recent observation [16] of a noticeable spread in arrival times for high-energy gamma rays from distant gamma-ray bursts has prompted the suggestion that it is unlikely that fuzziness of radio or optical images of distant extragalactic sources would be observed. The latter observation is exactly what this paper is about, thus we need to show that we disagree with the suggestion. Our detailed argument (based on previous work [17]) is given in Sec. III.

In Sec. IV, we present a more detailed discussion of wave-vector uncertainty in spacetime foam models. We discuss specifics of the necessary null tests for spacetime foam models as well as the reasons why spacetime foam halos cannot be interpreted as resulting from multiple scattering events.

So far, in our attempts to detect spacetime foam, only the HST images of a few quasars/AGNs [5,18] have been analyzed [3,4,6,15]. In Sec. V, we show the size of expected spacetime foam broadening for various telescopes in a variety of wavebands. We then concentrate on the optical regime. Noting that the VLTI will not be in full operation for some time, we concentrate our attention in this paper on an analysis of quasar images in the HST archive. This is done in Sec. VI. We discuss results and conclusions in Sec. VII.

II. DISTANCE FLUCTUATION EXPRESSION

In this section, we will calculate the numerical factor N in the distance fluctuation expression for $\delta l \gtrsim N l_P^\alpha l^{1-\alpha}$.

(a) For the random-walk model with step length l_P, taking M steps with a probability $p(q)$ of taking a forward (backward) step, the mean square displacement is given by $(\delta l)^2 = 4Mpql_P^2$. For the distance l, the number of steps is $M = l/l_P$. Therefore, with an unbiased random-walk, $p = q = 1/2$, we get an root-mean-square displacement of $\delta l = l^{1/2}l_P^{1/2}$, so $N = 1$.

(b) Obviously for the anticorrelation model, since δl is always equal to l_P, again $N = 1$.

(c) For the holographic model, we now have an explicit calculation which sets narrow limits for N. We use four different methods and their consistency with each other (to within a factor of 2 or so, as we will show) bodes well for the robustness of our result. The ingredients behind all the approaches are black hole physics and quantum mechanics.

A. Quantum computation

This method [19,20] relies on the fact that quantum fluctuations of spacetime manifest themselves in the form of uncertainties in the geometry of spacetime. Hence the structure of spacetime foam can be inferred from the accuracy with which we can measure that geometry. Let us consider mapping out the geometry of spacetime for a spherical volume of radius l over the amount of time $T = 2l/c$ it takes light to cross the volume. One way to do this is to fill the space with clocks, exchanging signals with other clocks and measuring the signals' times of arrival. This process of mapping the geometry of spacetime is a kind of computation, in which distances are gauged by transmitting and processing information. The total number of operations, including the ticks of the clocks and the measurements of signals, is bounded by the Margolus-Levitin theorem [21] in quantum computation, which stipulates that the rate of operations for any computer cannot exceed the amount of energy E that is available for computation divided by $\pi\hbar/2$. A total mass M of clocks then yields, via the Margolus-Levitin theorem, the bound on the total number of operations given by $(2Mc^2/\pi\hbar) \times 2l/c$. But to prevent black hole formation, M must be less than $lc^2/2G$. Together, these two limits imply that the total number of operations that can occur in a spatial volume of radius l for a time period $2l/c$ is no greater than $2(l/l_P)^2/\pi$. To maximize spatial resolution, each clock must tick only once during the entire time period. If we

regard the operations partitioning the spacetime volume into "cells", then on the average each cell occupies a spatial volume no less than $(4\pi l^3/3)/(2l^2/\pi l_P^2) = 2\pi^2 l l_P^2/3$, yielding an average separation between neighboring cells no less than $(2\pi^2/3)^{1/3} l^{1/3} l_P^{2/3}$. This spatial separation is interpreted as the average minimum uncertainty in the measurement of a distance l, that is, $\delta l \gtrsim 1.9 l^{1/3} l_P^{2/3}$; thus, $N = 1.9$.

B. Heisenberg's uncertainty principle

This method involves an estimate of the maximum number of (massless) particles that can be put inside a spherical region of radius l. Heisenberg's uncertainty principle can be invoked to give the minimum momentum of each particle to be $\frac{1}{2} \times (\hbar/2l)$, or in other words, the minimum energy of each particle is no less than $\frac{1}{4} \times \hbar c/l$. To prevent black hole formation, the total energy is bounded by $\frac{1}{2} \times lc^4/G$. Thus the total number of particles is no greater than $2(l/l_P)^2$. This yields $\delta l \gtrsim (\frac{2\pi}{3})^{1/3} \times l^{1/3} l_P^{2/3} = 1.3 l^{1/3} l_P^{2/3}$; thus, $N = 1.3$.

C. Holographic principle

This method [22,23] is based on the upper bound on the number I of degrees of freedom that can be put in a spherical volume of radius l. According to the holographic principle,[11,12] the entropy S in the sphere is bounded by $S/k_B \lesssim \frac{1}{4} 4\pi l^2/l_P^2$, where k_B is the Boltzman constant. Recalling that $e^{S/k_B} = 2^I$, we get $I \lesssim \pi(l/l_P)^2/\ln 2$. The average separation between neighboring degrees of freedom then yields $\delta l \gtrsim (\frac{4\ln 2}{3})^{1/3} l^{1/3} l_P^{2/3} = 0.97 l^{1/3} l_P^{2/3}$; thus, $N = 0.97$.

D. The Wigner-Salecker gedanken experiment

In this method [9,10,24,25] we conduct an ideal thought experiment to measure a distance l between a clock and a mirror, By sending a light signal from the clock to the mirror in a timing experiment, we can determine l. The clock's and the mirror's positions jiggle according to Heisenberg's uncertainty principle, resulting in an uncertainty δl in the measurement of l.

Let us concentrate on the fluctuation of the distance l due to the jiggling of the clock's position. If the clock of mass m has a linear spread δl (and hence an uncertainty of speed, via Heisenberg's uncertainty principle, given by $\hbar/(2m\delta l)$) when the light signal leaves the clock, then its position spread grows to $\delta l + \hbar \frac{1}{2m\delta l} \frac{2l}{c}$ when the light signal returns to the clock, with the minimum at $\delta l = \hbar l/mc$. Thus, quantum mechanics alone would suggest using a massive clock. Now consider the clock to be light-clock consisting of a spherical cavity of diameter d, surrounded by a mirror wall between which bounces a beam of light. For the uncertainty in distance not to exceed δl, the clock must tick off time fast enough so that $d/c \lesssim \delta l/c$. But d must be larger than twice the Schwarzschild radius $2Gm/c^2$. These two requirements imply $\delta l \gtrsim 4Gm/c^2$ which combines with the requirement from quantum mechanics to yield $(\delta l)^3 \gtrsim 4l l_P^2$ (independent of the mass m of the clock), or $\delta l \gtrsim 1.6 l^{1/3} l_P^{2/3}$; thus, $N = 1.6$. A remark is in order: taking into account also the jiggling of the mirror's position can only enhance δl. As another remark, we note that the problem of distance measurement has been discussed in [26] in noncritical string theory.

Thus, all four different methods yield very similar results. (Part of the relatively small discrepancy can be traced to the mismatch between the geometries of spheres and cubes.) This is not surprising, as our result depends not on any particular theory of quantum gravity, but only on the quantum nature of measurements. In the discussion below, we will use the preceding arguments to set the allowable range for N in the holographic model as: $0.97 \leq N \leq 1.9$.

III. SPREAD IN ARRIVAL TIMES FROM DISTANT PULSED SOURCES

In this section we will discuss the technique of using the spread in arrival times of photons as a possible technique for detecting spacetime foam. We are motivated by the interesting detection of a minimal spread in the arrival times of high-energy photons from distant GRB reported by [16]. While useful in putting a limit on the variation of the speed of light of a definite sign, this technique is far less useful than the measured angular size in constraining the degree of fuzziness of spacetime in the spacetime foam models that we consider in this paper. The reason is that spacetime foam models predict that the speed of light fluctuates (i.e., the fluctuation takes on $\pm$sign with equal probability): at one instant a particular photon is faster than the average of the other photons, but at the next instant it is slower. We will show that the cumulative effect of the fluctuations is too small to be detectable [17], even for high-energy gamma rays that have travelled ~7 billion light-years halfway across the Universe [16], for most of the spacetime foam models.

First we need to examine the cumulative effects [4] of spacetime fluctuations over a large distance. Consider a distance l, and divide it into l/λ equal parts each of which has length λ (λ can be as small as l_P). If we start with $\delta\lambda$ from each part, the question is how do the l/λ parts add up to δl for the whole distance l. In other words, we want to find the cumulative factor $\mathcal{C}$ defined by $\delta l = \mathcal{C}\delta\lambda$, Since $\delta l \sim l^{1-\alpha} l_P^\alpha$ and $\delta\lambda \sim \lambda^{1-\alpha} l_P^\alpha$, the result is $\mathcal{C} = (\frac{l}{\lambda})^{1-\alpha}$. Note that the cumulative factor is *not* linear in (l/λ), i.e., $\frac{\delta l}{\delta\lambda} \neq \frac{l}{\lambda}$. (In fact, it is much smaller than l/λ). The reason for this is obvious: the $\delta\lambda$'s from the l/λ parts in l do *not* add coherently.

Next we have to find how much the speed of light fluctuates. We proceed as follows: Just as there are uncertainties in spacetime measurements, there are also uncer-

tainties in energy-momentum measurements due to space-time foam effects. Thus there is a limit to how accurately we can measure and know the energy and momentum of a system [9,10]. Imagine sending a particle of momentum p to probe a certain structure of spatial extent l so that $p \sim \hbar/l$. It follows that $\delta p \sim (\hbar/l^2)\delta l$. Spacetime fluctuations $\delta l \gtrsim l(l_P/l)^\alpha$ can now be used to give

$$\delta p \sim p\left(\frac{p}{m_P c}\right)^\alpha. \qquad (2)$$

The corresponding statement for energy uncertainties is

$$\delta E \sim E\left(\frac{E}{E_P}\right)^\alpha. \qquad (3)$$

Here m_P and $E_P = m_P c^2$ denote the Planck mass and energy, respectively. These energy-momentum uncertainties modify the dispersion relation for the photons to read:

$$E^2 \simeq c^2 p^2 + \epsilon E^2\left(\frac{E}{E_P}\right)^\alpha, \qquad (4)$$

where $\epsilon \sim \pm 1$. Thus the speed of light $v = \frac{\partial E}{\partial p}$ fluctuates by

$$\delta v \sim 2\epsilon c(E/E_P)^\alpha. \qquad (5)$$

We emphasize that all the fluctuations take on $\pm$sign with equal probability (like a Gaussian distribution about c).

It follows from the above discussion that for photons emitted simultaneously from a distant source coming towards our detector, we would expect an energy-dependent spread in their arrival times. To maximize the spread in arrival times, we should look for energetic photons from distant sources. So the idea is to look for a noticeable spread in arrival times for such high-energy gamma rays from distant gamma-ray bursts. This proposal was first made by [28] in another context.

To underscore the importance of using the correct cumulative factor to estimate the spacetime foam effect, let us first proceed in a naive manner. At first sight, the fluctuating speed of light would *seem* to yield an energy-dependent spread in the arrival times of photons of energy E given by $\delta t \sim \delta v(l/c^2) \sim t(E/E_P)^\alpha$, where $t = l/c$ is the average overall time of travel from the photon source (distance l away). But these results for the spread of arrival times of photons are *not* correct, because we have inadvertently used $l/\lambda \sim Et/\hbar$ as the cumulative factor instead of the correct factor $(l/\lambda)^{1-\alpha} \sim (Et/\hbar)^{1-\alpha}$. Using the correct cumulative factor, we get a much smaller

$$\delta t \sim t^{1-\alpha} t_P^\alpha \sim \delta l/c \qquad (6)$$

for the spread in arrival time of the photons [17], independent of energy E (or photon wavelength, λ). Here $t_P \sim 10^{-44}$ sec is the minuscule Planck time. Thus, the result is that the time-of-flight differences increase only with the $(1 - \alpha)$-power of the average overall time of

travel $t = l/c$ from the gamma-ray bursts to our detector, leading to a time spread too small to be detectable (except for the uninteresting range of α close to 0).

The new Fermi Gamma-ray Space Telescope results [16] of $\delta t \lesssim 1$ s for $t \sim 7$ billion years, rule out only spacetime foam models with $\alpha \lesssim 0.3$. We note that the result $\delta t \gtrsim t^{1-\alpha} t_P^\alpha$ is to be expected if we recall that the spread of arrival times can be traced to uncertainty in the distance that the photons have travelled from the distant source to our telescopes. In other words, gamma-ray arrival time dispersions ~ 1 s from sources at distances $\sim 7 \times 10^9$ ly only reject spacetime foam models in which the effects almost add coherently ($0 \leq \alpha < 0.3$) but do not test the major models discussed above (i.e., $\alpha = 1/2, 2/3, 1$). For example, the holographic model predicts an energy-independent dispersion of arrival times $\sim 2.5 \times 10^{-24}$ s.

Finally, in the following section on spacetime foam-induced uncertainties in wave-vector direction, we show angular uncertainties in the wave-vector direction are not the result of random multiple scattering events which could, in principle, lead to much larger uncertainty in arrival times.

IV. ANGULAR FLUCTUATIONS: MEASUREMENT

At the outset it must be reemphasized that the test for spacetime foam effects is a null test. A theoretical model for spacetime foam is disproved if images of a distant point source do not exhibit the blurring predicted by theoretical spacetime foam models.

As discussed in the Introduction, the fundamental uncertainties caused by spacetime foam are spatial, not angular. Strictly speaking, the models specify the uncertainty $\pm \delta l$, in distance between a source and observer along the line of sight. This is because δl is defined by the uncertainty in the distance measured by light travel times. Straightforward extensions of the models hypothesize that δl is isotropic in the sense that the uncertainty perpendicular to the line of sight is equal to the line-of-sight uncertainty (cf. CNvD, 2006). Of course, there is also a corresponding uncertainty in the transit time for light from source to observer, $\delta t \sim \delta l/c$, which was discussed in Sec. III. Furthermore, since the globally averaged wave front is effectively spherical, it implies that globally averaged photon trajectories deviate from the direct line of sight by an angle less than or equal to $\delta l/l$. A direct consequence of this limitation on the globally averaged angular deflection of photon trajectories is that the theoretically expected blurring of distant images due to spacetime foam is not the result of a random walk of small angle photon scatterings along the line of sight, since the uncertainties in the derived directions of the local wave vectors must result in the same spatial uncertainty, δl (no matter how many wave crests pass the observer's location). For example, in the "thin screen approximation", the accumulated transverse path of multiply scattered photons is

approximated as $(\delta\psi)l \gg \delta l$. This would lead to expected time lags, $\delta\psi(l/c) \gg \delta l/c$, in conflict with the basic premises for space time foam models.

The reasons why a straightforward application of standard small angle scattering theory as discussed in [27](e.g., gravitational micro-lensing) is not applicable are two-fold:

(1) the "scattering centers" for spacetime foam would be virtual Planck masses that exist for only a Planck time ($\sim 10^{-44}$ sec) which is much less than the period ($\sim 10^{-28}$ sec) of even the highest energy (TeV) detectable gamma rays.

(2) the "density" of such virtual scattering centers can only be inferred from nonlocal theories such as the holographic principle.

However, according to theory, although the wave front remains approximately spherical its precise location and structure is best characterized as a "cloud" of uncertainty whose scale is δl. These uncertainties are not realized as fluctuations until physical measurements are performed. This is consistent with the quantum physics of these models with their reliance on the quantum Uncertainty Principle.

As the light wave encounters a "detector" (e.g. a telescope) the spatial uncertainty shows up as a random series of fluctuations of scale $\leq (\pm)\delta x$ along and perpendicular to the line of sight causing fluctuations (i.e. "jitter") in the apparent angular direction of the wave vector recorded by the detector. However, the cloud of uncertainty associated with these spacetime foam models requires that the spatial uncertainties in the wave, from crest to crest, do not continuously connect. This cloud of uncertainties is chaotic and fluctuations are not correlated from crest to crest. That is, you cannot trace caustics from one crest to another.

Furthermore, it must be understood that a necessary condition for measurement of angular blurring requires that $\delta l \ll \lambda$, which corresponds to the limit for quantum coherence. As the electromagnetic wave from the extragalactic source propagates, the phase uncertainty $\Delta\phi \sim 2\pi\delta l/\lambda$ gets larger. Once $\Delta\phi \sim 2\pi$ (corresponding to $\delta l \sim \lambda$), quantum coherence is lost. At this point, while the amplitude of the electromagnetic wave remains intact, all phase information is lost. The distance at which spacetime foam-induced decoherence sets in depends on the model. For the "α-models," coherence is lost sooner when α is smaller.

In the realm where imaging is possible ($\delta l \ll \lambda$), detecting spacetime foam effects via "blurring" must involve a form of triangulation by comparing δl with some well-defined localized length scale, B, that would allow for the measurement of an angular uncertainty defined by the dimensionless ratio, $\delta\psi \sim \delta l/B$. Possible length scales defining B that may be relevant are: 1) the diameter of the telescope, D, or 2) the wavelength of the radiation, λ. In both cases, the angular uncertainty would represent the theoretically predicted apparent broadening of the image

of a point source of radiation caused by spacetime foam as recorded by a telescope plus detector.

GEOMETRIC OPTICS:

If the telescope/detector does not record phase information, then angular broadening at the focal plane will be determined by ray-tracing. Therefore, the spatial uncertainty, δl, in the location of a ray on the primary (whether it is a lens or a mirror), will result in an angular uncertainty, at the focal plane of

$$\delta\psi|_{\text{GeometricOptics}} \sim \delta\psi|_{\text{min}} \sim 2\delta l/D \ll \lambda/D. \quad (7)$$

(Of course the focal ratio of the telescope also plays a role in the above equation, but the key parameter is the size of the primary.) When combined with the requirement for quantum coherence discussed above (i.e., $\delta l \ll \lambda$), Eq. (7) virtually guarantees that spacetime foam effects will be undetectable by techniques that are phase insensitive (i.e. geometric optics).

WAVE OPTICS:

Clearly, the largest measurable angular effect would be associated with using the shortest length standard, i.e. the wavelength. As stated previously, the only way to accomplish such a measurement is via interference techniques such as diffraction-limited imaging and/or interferometry. In this case, since $\delta l = Nl^{(1-\alpha)}l_P^\alpha$, the angular uncertainty (i.e. the blurring angle) is

$$\delta\psi|_{\text{WaveOptics}} = \delta\psi_{\text{max}} = \delta l/\lambda = N(l/\lambda)^{(1-\alpha)}(l_P/\lambda)^\alpha. \quad (8)$$

This relation is identical in form to the relation defining δl, with dimensionless ratios, $(l, l_P)/\lambda$, replacing the previously defined distances. Note the so-called "accumulation factor," $(l/\lambda)^{(1-\alpha)}$, plays the same role as discussed previously in the growth of the distance uncertainty and the time uncertainty discussed in Sec. III. The magnitude of $\delta\psi$ as given in Eq. (8) is consistent with our assumption of isotropic fluctuations which implies comparable sizes of the wave-vector fluctuations perpendicular (δk_{perp}) to and along (δk_{par}) the line of sight (cf. CNvD, 2006). To wit, the size of the angular spread $\delta\psi$ is given by $\Sigma\delta k_{\text{perp}}/k$ where Σ stands for summation over the l/λ intervals each of length λ. Since $\delta k_{\text{perp}} \sim \delta k_{\text{par}}$ according to the assumption of isotropic fluctuations and $k_{\text{par}} \approx k = 2\pi/\lambda$, we have $\delta\psi \sim \Sigma\delta k/k = \Sigma\delta\lambda/\lambda \sim \delta l/\lambda$.

Thus, interference techniques offer the best (perhaps only) method for testing for the presence of spacetime foam because the observed wavelength offers the shortest line of sight baseline calibrator for measuring the local angular uncertainty in wave-vector direction and interference is the only way to exploit the wavelength as a calibrator. That is, the expected blurring of diffraction-limited images is a consequence of interference effects resulting from wave-front "distortions" (or "measurement errors") corresponding to ratios of positional uncertainties of order

$\pm \delta l$ along, and perpendicular to, the line of sight and the corresponding angular uncertainties $\pm \delta l/\lambda$. In particular, the angular uncertainty corresponds to the "wave-front errors" that are the basis for calculating Strehl ratios in wave optics. Since the Strehl ratio is designed to provide a quantitative measure of the departures from diffraction-limited optics, the technique is well suited for providing the proposed null test of spacetime foam models. Simply put, if distant point sources do not show reductions in Strehl ratios predicted by theoretical models, the model must be rejected. The application of this technique is discussed in detail in Sec. VI below.

We end this section with a summary of what we expect a telescope would observe at different locations. As the electromagnetic wave from the extragalactic source propagates, the phase uncertainty $\Delta \phi \sim 2\pi \delta l/\lambda$ gets larger. So long as $\Delta \phi \ll \lambda/D$ (in other words, so long as $\delta l \ll \lambda^2/D$), normal interference pattern is observed. Farther from the source, as $\Delta \phi \sim \lambda/D$ (i.e., $\delta l \sim \lambda^2/D$), we expect the interference pattern to be replaced by a halo structure. But once $\Delta \phi$ reaches $\sim 2\pi$ (corresponding to $\delta l \sim \lambda$), quantum coherence is lost, and the images will become all blurred. At this point, while the amplitude of the electromagnetic wave remains intact, all phase information is lost. How far from the source these different stages (from interference pattern to halo structure to all blurred images) are encountered, of course, depends on the different spacetime foam models. For example, for the AGN PKS 1413+135 [18], the random-walk model predicts that $\Delta \phi \sim 10 \times 2\pi$, while the holographic model yields $\Delta \phi \sim 10^{-9} \times 2\pi$ for $\lambda \approx 1.6 \ \mu$m [6]. Thus, according to the random-walk model, $\Delta \phi$ has reached the stage beyond the quantum coherence limit and hence the image should be all blurred. However, even supplemented with the assumption of isotropic fluctuations (viz., $\delta k_{\text{perp}} \sim \delta k_{\text{par}}$) which henceforth we adopt, the holographic model predicts that a normal interference pattern is observed at the HST (with $D \approx 2.4$ m) for $\lambda \approx 1.6 \ \mu$m. On the other hand, if D were about 3 orders of magnitude larger, according to the holographic model, a halo structure would be observed.

V. TESTING SPACETIME FOAM MODELS USING ASTRONOMICAL OBSERVATIONS

With the above as background, we are now prepared to discuss the issue of testing spacetime foam models. This subject has been discussed previously by CNvD as well as [5,15].

CNvD described a more flexible way to use astronomical observations, which has been summarized and expanded upon in the preceding sections. As we note in the Introduction, for point sources of low redshift z, it is not so critical which distance expressions for the point sources one should use. But for high-redshift objects, it does make a difference. We have already argued that the appropriate

cosmological distance to use is the total line-of-sight co-moving distance [14] given by

$$D_C(z) = D_H \int_0^z dz'/E(z'), \qquad (9)$$

where

$$E(z) = \sqrt{\Omega_M(1+z)^3 + \Omega_k(1+z)^2 + \Omega_\Lambda}, \qquad (10)$$

with $D_H = c/H_0$ being the Hubble distance, Ω_M, Ω_k and Ω_Λ being the (fractional) density parameter associated with matter, curvature and the cosmological constant, respectively. Consistent with the latest Wilkinson Microwave Anisotropy Probe (WMAP) cosmic microwave background (CMB) data, we will use $\Omega_M = 0.25$, $\Omega_\Lambda = 0.75$ and $\Omega_k = 0$, and for the Hubble distance we will use $D_H = 1.3 \times 10^{26}$ meters. In terms of the comoving distance, for the various models of spacetime foam (parametrized by α), the equivalent halo size is given by

$$\delta \psi = N(1-\alpha) l_P^\alpha D_H^{1-\alpha} I(z, \alpha)/\lambda_o, \qquad (11)$$

with

$$I(z, \alpha) = \int_0^z dz'(1+z')/(E(z')) \left(\int_0^{z'} dz''/E(z'') \right)^{-\alpha}, \quad (12)$$

where the factor $(1+z')$ in the integral corrects the observed wavelength λ_o, back to the wavelength $\lambda(z')$ at redshift z'. That is $\lambda(z') = \lambda_o/(1+z')$. We have used these results to produce Fig. 1, which shows the predictions made for three different values of α, i.e. $\alpha = 2/3$, 0.6, 1/2 respectively, for the size of observed haloes produced by accumulated phase dispersion for a source at two redshifts, respectively $z = 4$ and $z = 1$. This graph plots wavelengths from hard x-rays (equivalent photon energy $\sim$100 keV) down to radio waves. The labeled arrows pointing upward to the right delineate the diffraction-limited response of various existing or proposed telescopes. That is, with the exception of *Chandra*, the arrows plot λ_o/D, where D is the aperture/baseline length and the length of the arrow is determined by the telescope's wavelength limits. The shallower slope of *Chandra's* results from its grazing-incident optics and its complicated point spread function.

As $\delta \psi$ depends nontrivially on the redshift of the source, a remark on the effect of the uncertainties in the determination of the sources is in order. We have calculated the ratio $\delta I/I$ for a variety of redshifts and uncertainties. Some sample values are given in Table I. As can be seen, the effect is small, unless the uncertainty in the redshift, δz, grows significantly larger than 0.1, as would be the case for photometric redshift determinations [29,30]

Steinbring [15] showed a plot of a somewhat similar nature based, however, on luminosity distance rather than the comoving distance (his Fig. 1). The main differences here are corrected curves for $\alpha = 2/3$ and 1/2, since [15] also did not show the curves yielded by CNvD.
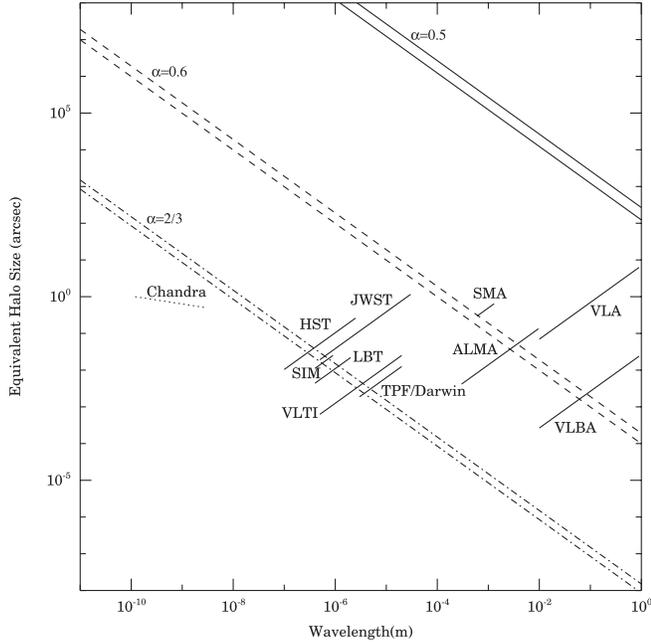
FIG. 1. The detectability of various models of foamy space-time with existing and planned telescopes. Diagonal tracks are shown for three models of foamy spacetime, namely $\alpha = 0.5$, 0.6, 2/3, for $z = 1$ and 4 (respectively the lower and upper tracks for each model) and $N = 1.9$. Also shown are the observing ranges and theoretical resolution limits (i.e., PSF size) for a wide variety of telescopes, both current and planned. The tracks for each telescope represent the diffraction limit with the exception of the dotted track for *Chandra*, whose complicated PSF is NOT diffraction-limited (see Sec. V). As such, they represent the detectability limit for these observations, in the case of a perfect telescope of that size. Importantly, note that in practical terms a given telescope may not be able to probe quite as far as pictured, as in the final analysis the region probed is also a function of Strehl ratio (see Sec. VI).

We note that if the arrow representing a telescope's diffraction-limited response lies *below* the halo size curve for a given α, that model may be excluded by observations. For example, as mentioned previously, the random-walk model ($\alpha = 1/2$) is clearly excluded by HST observations, as well as radio observations by the National Radio Astronomy Observatory Very Long Baseline Array. The

TABLE I.   Sample Uncertainties in I.

z	δz	α	$\delta I(z, \alpha)/I(z, \alpha)$
1.00	0.01	0.50	0.0104
1.00	0.01	0.60	0.0101
1.00	0.01	0.67	0.0099
5.00	0.01	0.50	0.0018
5.00	0.01	0.60	0.0013
5.00	0.01	0.67	0.0011
5.00	0.05	0.50	0.0090
5.00	0.05	0.60	0.0067
5.00	0.05	0.67	0.0055

latter surveys find numerous examples of unresolved sources at cosmological redshifts [31,32]. We also note that HST observations at short wavelengths ($\sim 10^{-6}$–10^{-7} m) appear to be capable of testing the holographic model ($\alpha = 2/3$) and certainly may exclude $\alpha = 0.6$.

Before delving further into the observational record to discuss what models of spacetime foam are excluded by the current data, it is useful to make a few comments. First of all, what types of observations and objects would be useful for constraining or rejecting spacetime foam models? In principle, all one needs are high-resolution imaging observations of a source that is unresolved and at high redshift. However, as noted previously, for a variety of practical reasons the source must be reasonably bright. This is for two reasons. First, one needs to be able to reliably distinguish a halo produced by dispersions induced by quantum fluctuations in spacetime, from a faint "halo" that might be due to intrinsic structure in the source. For example, in the optical, every bright extragalactic point source, be it a supernova, quasar (QSO), GRB or otherwise, is resident in a galaxy, which could very easily mimic or disguise a halo. Thus, one wants to be able to achieve large dynamic ranges (at least hundreds or thousands to one) on the image with a reasonable amount of integration time. This host galaxy can also scatter light from the AGN, so that there may still be some halo left in the image (e.g., [33]). However, the scattered light is polarized, so that there is a clear way to discriminate the effects of spacetime foam from scattering effects. Secondly, a number of observing methods, particularly optical interferometry, require much brighter sources in order to be able to find fringes in real time. For example, the design of the VLTI requires sources in the IR K-band brighter than 14th magnitude. Folding these constraints in, for noninterferometric observations in the optical, any bright point source will do, be it a QSO or GRB. Unfortunately, SN Ia or SN II cannot be used, as they are comparable in luminosity to the host galaxy so they will not allow large enough signal to noise to be reached (i.e., we will not be able to distinguish structure in the host galaxy from broadening due to space-time foam). However, for optical interferometers such as the VLTI or (in the future) the Space Interferometry Mission (SIM) or Darwin/Terrestrial Planet Finder, only the brightest blazars observed in outburst, or the prompt flash of a powerful GRB will do.

In the radio, any bright QSO or BL Lac object will suffice, and fortunately there are large numbers of these. A large number have been found to have unresolved sources, as seen with both the National Radio Astronomy Observatory Very Large Array and Very Long Baseline Array [31,32]. These observations confirm at radio wavelengths that the random-walk model can be ruled out. None of these observations have sufficient resolution to test the holographic model, however.

Ideally, one wants to observe with any telescope that will yield the smallest λ/D ratio as the diffraction limit would then dictate that one could set the smallest limit on the size of any halo corresponding to the wavelength at which a given spacetime foam model would predict the largest halo size. However, for one of the telescopes shown on Fig. 1, namely, the *Chandra* X-ray Observatory, this is not the case. Unlike the radio, IR and optical telescopes shown there, *Chandra*'s optical design is governed by the short wavelengths (comparable to interatom spacings) of x-ray photons, which make ordinary normal-incidence optics impractical. Instead, *Chandra* uses grazing incidence mirrors in a nested [34,35] design. In this design, it is the nesting of the mirrors that focuses the light on the imaging plane. As a result, the point spread function (PSF) is not diffraction-limited, and the telescope cannot sense the wave front coherently. We have plotted *Chandra*'s angular resolution in Fig. 1 using parameters from the *Chandra Proposer's Observatory Guide*, using values corresponding to the 75% level in the encircled energy function (see specifically Figures 4.6 and 4.7). However, in Fig. 1 we show the *Chandra* line as dotted. This is because its inability to sense the wave front coherently makes it unsuitable for testing models of spacetime foam because the blurring of the images is a product of interference effects rather than photon scattering, an effect which non-diffraction-limited optics are not sensitive to (see Sec. IV).

Of course one would also like to be able to obtain constraints in as many bands as possible, since finding the halo size as a function of frequency, in principle, allows one to search for the characteristic λ^{-1} dependence in the size of the spacetime foam scattering disk (discussed in Sec. IV). Constraints obtained in only one band are susceptible to bias by structure intrinsic to the source (host galaxy or extended emission line regions, for example) or to the PSF of that band

With the above provisos, then, we can now discuss the constraints that can currently be put on spacetime foam models. It is apparent that, with current telescopes, all spacetime models with $\alpha \leq 0.6$ are firmly excluded by the combined archives of telescopes in the optical, radio and x-ray where unresolved sources have, at some level (see below) been observed at every redshift up to at least $z = 5$. With HST observations, this constraint can be significantly tightened. Thus the random-walk ($\alpha = 1/2$) model is securely excluded at very high confidence, as in fact are all models with $\alpha \leq 0.65$. The Holographic ($\alpha = 2/3$) model is very close to being tested and will enter that regime once the VLTI is fully operational, and may be tested by HST in the ultraviolet.

VI. TESTING SPACETIME FOAM MODELS—THE HST QUASAR ARCHIVE

Because the Strehl ratio is defined as the ratio of the observed image peak to the peak diffraction spike of an unabberated telescope, it provides a useful way to assess the effects of spacetime foam. As discussed above, spacetime foam causes wave-front "errors" in the images of distant point sources. The effect is similar to atmospheric "seeing" and, in fact, we follow the general analysis of Sandler *et al.* [36] for the degradation of Strehl ratios resulting from wave-front errors. Since spacetime foam-induced wave-front errors are not spatially correlated, a simple approximation for the degraded Strehl ratio is [36]

$$S_{\text{Obs}} = S_M \exp[-(\sigma_I^2 + \sigma_\phi^2)] \qquad (13)$$

where $S_M \leq 1$ represents a degradation of the observed Strehl ratio due to masking effects (which may or may not be spatially correlated as discussed above), σ_I represents uncorrelated wave-front errors induced by the instrumentation (i.e., telescope plus instruments) and σ_ϕ represents uncorrelated wave-front errors induced by spacetime foam. Both of these dispersions are expressed in units of the telescope's diffraction limit, λ/D. For convenience we then define the spacetime foam-degraded Strehl S_ϕ as:

$$S_\phi = \exp(-\sigma_\phi^2) \qquad (14)$$

where σ_ϕ is simply the angular dispersion of the wave-front vector due to external effects (i.e., $\delta\psi$ in Eq. (11)) divided by λ/D,

$$\sigma_\phi = N(1 - \alpha)l_P^\alpha D_H^{1-\alpha} I(z, \alpha)D/\lambda_o^2. \qquad (15)$$

($S_\phi \sim 1$, of course, corresponds to no image degradation.) This approximation, of course, breaks down when $\sigma_\phi \sim 1$, i.e., when the wave front angular dispersion is comparable to the telescope's resolution. A fully parametrized version of the resultant Strehl ratio then is

$$S_\phi = \exp(-N^2(1 - \alpha)^2 l_P^{2\alpha} D_H^{2(1-\alpha)} I^2(z, \alpha)D^2/\lambda_o^4). \qquad (16)$$

A few comments concerning parameter sensitivity of these models for Strehl ratio are in order:

(1) The model Strehl ratio is strongly sensitive to wavelength.

(2) Although we have managed (Sec. II) to narrow the range of possible values for the constant, N, in the holographic model the remaining uncertainty in this parameter ($0.97 < N < 1.9$) leads to a factor of 3.4 in the argument of the Strehl ratio exponential.

(3) The instrumental contribution, $S(\sigma_I)$ can be measured using a true point source, for example, a star.

(4) The model Strehl ratio is also exquisitely sensitive to the value of α.

Figure 2 illustrates the sensitivity to degradation of S_ϕ from spacetime foam as a function of redshift and of wavelength for α values of 2/3 (in black) and 0.655 (in grey)—assuming $N = 1.9$ in each case. In the left-hand figure we illustrate the change in S_ϕ expected for a point source with varying distance for three fixed wavelength values. In the right-hand figure, we show the change in S_ϕ
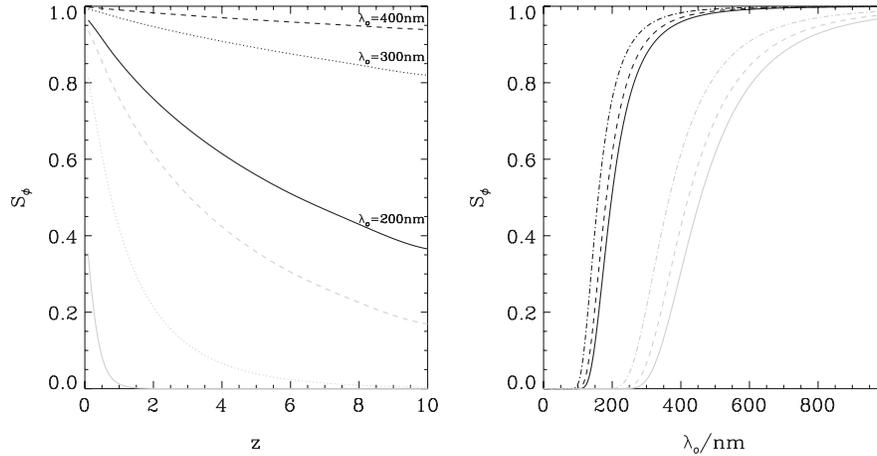
FIG. 2. Expected Strehl ratio with redshift (left) and wavelength (right) for two spacetime foam cases: $\alpha = 2/3$, $N = 1.9$ (black lines); $\alpha = 0.655$, $N = 1.9$ (grey lines). In the left-hand figure we illustrate the change in Strehl ratio expected for a point source with varying distance, z, for three fixed observed wavelengths ($\lambda_o = 200$, 300 and 400 nm as marked). In the right-hand figure we show the change in Strehl ratio expected for a point source at various three fixed distances: $z = 6$ (solid line), $z = 4$ (dashed line) and $z = 2$ (dot dashed line).

expected for a point source with varying wavelength at three fixed distances. We can see that HST is just able to probe the $\alpha = 2/3$ case at the very shortest (uv) wavelengths in its spectral range. We note that $N = 0.97$ shifts the curves in the left-hand figure to the right (i.e., increasing redshift). We also note that shorter wavelength is a greater imperative than increased distance for improving sensitivity to α. However, optical measurements may rule out lower values of α. Clearly the realm for testing the holographic model lies in redshifts $z \gg 1$. Notice, also, that even a modestly smaller value of $\alpha = .64$ clearly can be tested at redshifts more than an order of magnitude smaller.

To test the spacetime foam models using Strehl ratios, we explored the HST archive (http://archive.stsci.edu/hst/search.php) for observations of high-redshift quasars, using STARVIEW to cross reference suitable catalogues with the archive database. We explored the Sloan Digital Sky Survey (SDSS) DR5 quasar catalog [37] and a catalog of the highest redshift SDSS quasars [38] in addition to the quasar catalog of [39]—hereafter VCV. In Table II we present notable high-redshift quasars observed in the optical, near infrared, and uv using HST. We prioritize those observations that maximize the value of $I(z, \alpha)/\lambda_o$ (see Eq. (12)).

The current record for the highest redshift quasar is held by the Canada-France-Hawaii Telescope quasar survey: CFHQS J2329-0301 at $z = 6.43$. This has not yet been observed with HST. The highest redshift quasars with *HST* pointings all come from the SDSS, including SDSS J1030 +0524 at $z = 6.28$. and SDSS J1148+5251 at $z = 6.42$ The former was observed, along with other high-z SDSS quasars, using the *Advanced Camera for Surveys* (ACS) *High-Resolution Channel* (HRC) at $\lambda_o \sim 850$ nm by [38].

Blurring of these images has been studied inconclusively [15]. However, the observations are all at red wavelengths (F775W and F850LP), which impinges on their sensitivity to spacetime foam, especially the $\alpha = 2/3$ case (see Eq. (16), and Fig. 2). The latter was observed through two linear ramp filters by [41] at ~720 and ~900 nm, and by [42] in F850LP and F775W. Among other notable examples is the HDF-S QSO at $z = 2.24$ [44], which was observed as part of the multiwavelength coverage of the deep fields using the *Space Telescope Imaging Spectrograph* (STIS) in the ultraviolet. While offering the big advantage of shorter wavelengths, the STIS data is unsuitable for the present purpose due to the extreme distortion of the PSF, which appears triangular with no discernible Airy ring.

We were unable to find any short wavelength ($\lambda_o < 500$ nm) images of high-redshift ($z > 4$) quasars by cross-referencing with SDSS or VCV quasar catalogues. These short wavelength observations are critical because they represent the only range of the spectrum for which Fig. 1 indicates we may be able to probe the $\alpha = 2/3$ case.

We turned next to the Hubble Ultra-Deep Field (UDF). The UDF [46] is the deepest image taken of the sky to date. The 10^6 s long exposure was taken with the ACS using a multiangle dither pattern to smooth out the PSF. A number of intermediate-to-high-redshift quasars have since been identified in this field, with redshifts provided by the Grism ACS Program for Extragalactic Science (GRAPES) project [47]. A list of quasars in the UDF was published by [45]. Four such quasars were chosen as suitable candidates due to their relative isolation in the field (see Table II). While we acknowledge the UDF data is not ideal for this task, since the sources will be inherently faint, and the data is assembled in a complicated stacking procedure which may

TABLE II. Quasar pointings with high $I(z, \alpha)/\lambda_o$ (see Eq. (11)) values in the HST archive. $I(z, \alpha)/\lambda_o$ is a measure of the number of wavelengths travelled by the light detected at wavelength λ_o. All calculations in this table assume $\alpha = 2/3$.

Name	z	Instrument	Filter	λ_o [μm]	$I(z, \alpha)$	$I(z, \alpha)/\lambda_o$ [μm^{-1}]
SDSS J1044-0125 [15,38]	5.80	ACS/HRC	F850LP	0.91	6.98	7.71
SDSS J0836+0054 [15,38]	5.82	ACS/HRC	F850LP	0.91	6.99	7.72
SDSS J1306+0356 [15,38]	5.99	ACS/HRC	F850LP	0.91	7.06	7.81
SDSS J1030+0524 [15,38]	6.28	ACS/HRC	F850LP	0.91	7.19	7.95
SDSS J0913+5919 [15,40]	5.11	ACS/HRC	F775W	0.77	6.62	8.60
SDSS J2228-0757 [15,40]	5.14	ACS/HRC	F775W	0.77	6.64	8.62
SDSS J1208+0010 [15,40]	5.27	ACS/HRC	F775W	0.77	6.71	8.71
SDSS J0231-0728[15,40]	5.41	ACS/HRC	F775W	0.77	6.78	8.81
SDSS J1148+5251 [41]	6.42	ACS/WFC	FR716N-7220	0.72	7.26	10.08
SDSS J1148+5251 [41]	6.42	ACS/WFC	FR914M-9050	0.90	7.26	7.89
SDSS J1148+5251 [42]	6.42	ACS/WFC	F775W	0.77	7.26	9.42
SDSS J1148+5251 [42]	6.42	ACS/WFC	F850LP	0.91	7.26	8.02
SDSS J1048+4637 [42]	6.23	ACS/WFC	F775W	0.77	7.17	9.32
SDSS J1048+4637 [42]	6.23	ACS/WFC	F850LP	0.91	7.17	7.93
SDSS J1630+4012 [42]	6.05	ACS/WFC	F775W	0.77	7.09	9.21
SDSS J1630+4012 [42]	6.05	ACS/WFC	F850LP	0.91	7.09	7.84
4C 45.51 [43]	1.992	NICMOS	F165M	1.65	3.01	1.82
4C 45.51[a]	1.992	WFPC2	F814W	0.81	3.01	3.69
223338-603329 [44]	2.24	STIS/FUVMAMA	F25QTZ	0.16	3.56	22.27
HUDF QSO 4120 [45]	2.095	ACS/WFC	F435W	0.43	3.25	7.52
HUDF QSO 4120 [45]	2.095	ACS/WFC	F606W	0.59	3.25	5.50
HUDF QSO 4120 [45]	2.095	ACS/WFC	F775W	0.77	3.25	4.22
HUDF QSO 4120 [45]	2.095	ACS/WFC	F850LP	0.91	3.25	3.59
HUDF QSO 6732 [45]	3.193	ACS/WFC	F435W	0.43	5.08	11.76
HUDF QSO 6732 [45]	3.193	ACS/WFC	F606W	0.59	5.08	8.60
HUDF QSO 6732 [45]	3.193	ACS/WFC	F775W	0.77	5.08	6.60
HUDF QSO 6732 [45]	3.193	ACS/WFC	F850LP	0.91	5.08	5.61
HUDF QSO 9397 [45]	1.225	ACS/WFC	F435W	0.43	0.60	1.39
HUDF QSO 9397 [45]	1.225	ACS/WFC	F606W	0.59	0.60	1.02
HUDF QSO 9397 [45]	1.225	ACS/WFC	F775W	0.77	0.60	0.78
HUDF QSO 9397 [45]	1.225	ACS/WFC	F850LP	0.91	0.60	0.67
HUDF QSO 9487 [45]	4.094	ACS/WFC	F435W	0.43	5.96	13.79
HUDF QSO 9487 [45]	4.094	ACS/WFC	F606W	0.59	5.96	10.1
HUDF QSO 9487 [45]	4.094	ACS/WFC	F775W	0.77	5.96	7.74
HUDF QSO 9487 [45]	4.094	ACS/WFC	F850LP	0.91	5.96	6.58

[a]Floyd *et al.* (in preparation).

introduce smoothing, it is only nonideal in that it weakens our possibility of testing our null hypothesis: any smoothing effect serves to dilute the Strehl ratio further. It is clear from the table that the advantage of using shorter wavelength B-band data more than compensates for the lower redshift of the sources when compared to the SDSS quasars examined by [15]. Images of each UDF quasar in each band (B, V, i, and z), are presented in Fig. 3. It is noticeable, from the original UDF images, that HUDF-QSO 6732 appears somewhat blurred in the B filter (F435W).

As mentioned above, the Strehl ratio is defined as the ratio of the image peak to that of the diffraction spike of an unabberated telescope. The unaberrated PSF was calculated assuming a primary mirror radius of 1.2 m with an inner radius of 0.35 m, convolved with the filter-instrument response function at a resolution of 1 Å to produce an

unaberrated PSF for each filter. These are shown along with stellar PSF's for each band in Fig. 4. However, as discussed by [15], HST has a complicated non-azimuthally symmetric structure to its PSF due to the support structure of the telescope itself. This is partially mitigated by the UDF observing strategy, which smooths the PSF and makes it rounder. Furthermore, the processing that goes into the UDF removes the distortion present in raw images. Note that the signal-to-noise ratio of the quasars is too low to be able to obtain reliable photometry on the individual raw frames, which could be accurately compared to Tinytim image reduction models, as was done by [15]. We found it futile to model the UDF PSF using TinyTim due to the complicated stacking process (''drizzling''). Instead we resort to stellar PSF stars to produce ''corrected'' Strehl ratios (after Steinbring 2007). While we
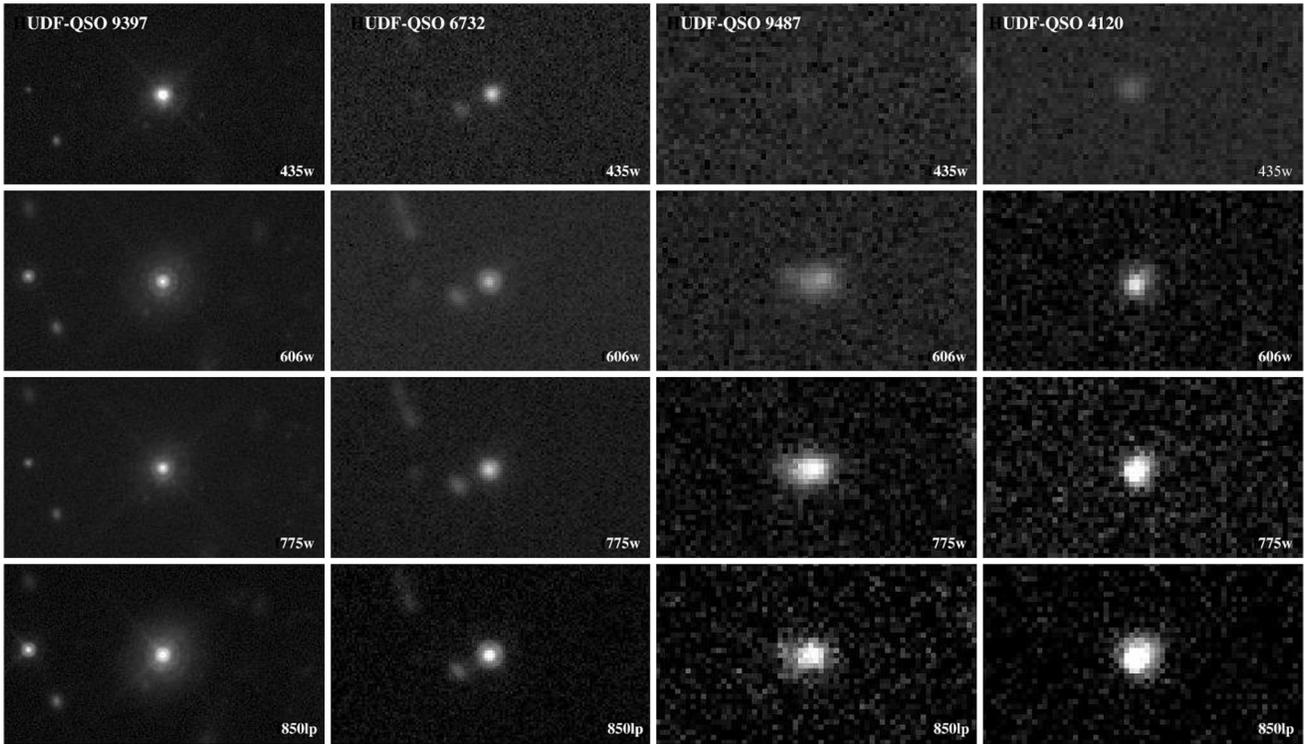
FIG. 3. The four HUDF quasars studied in this paper, from left to right: 9397 ($z = 1.2$); 6732 ($z = 3.2$); 9487 ($z = 4.1$); 4120 ($z = 2.1$). Descending rows show the F435W (B), F606W (V), F775W (I) and F850LP (x) images.
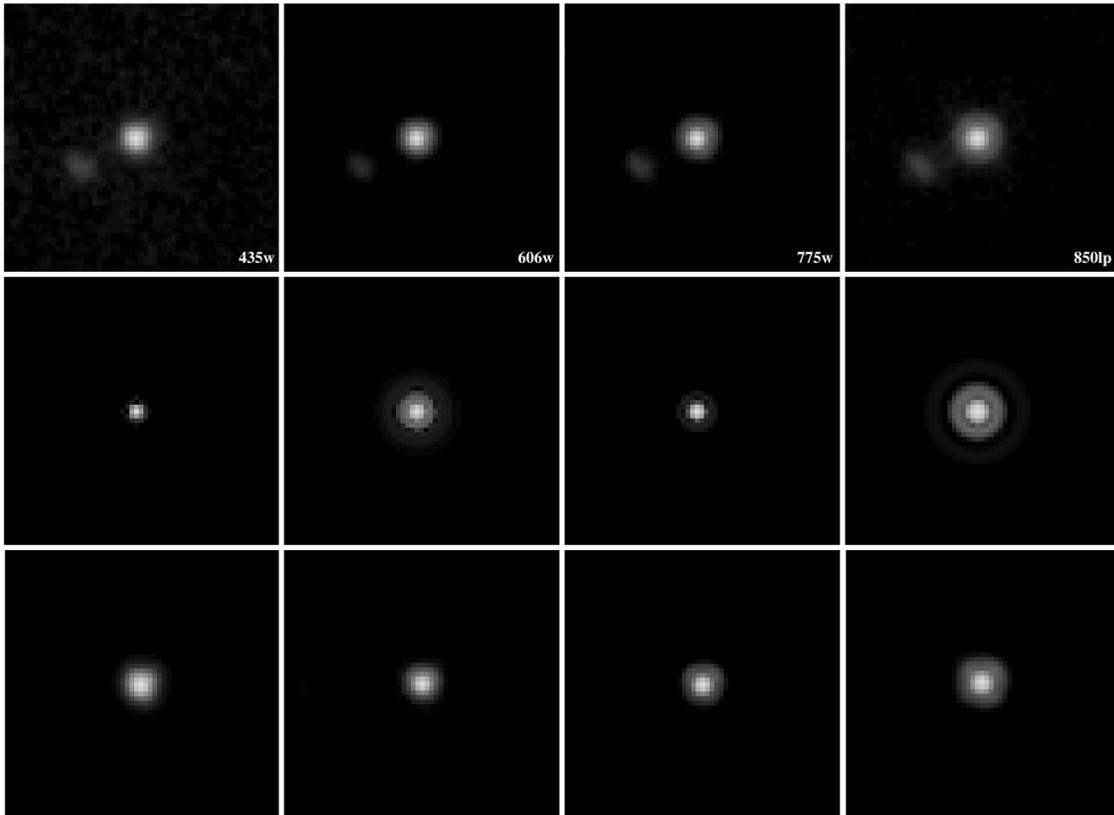

FIG. 4. Top, from left-to-right: HUDF-QSO 6732 in F435W (B), F606W (V), F775W (i) and F850LP (z) bands. Middle: The ideal model PSF (1.2 m radius mirror with central hole of 0.35 m radius) for same filters. Bottom: Stellar PSF's for the same filters.

TABLE III. Strehl ratios for UDF quasars (with identifier from [45]) and stars (with UDF coordinate positions) in each filter, with respect to the idealized, azimuthally symmetric PSF. Unmeasurable values occur where the image is saturated.

Source	F435W	F606W	F775W	F850LP
QSO 9397	0.31	0.40	0.60	0.60
QSO 6732	0.24	0.37	0.56	0.52
QSO 9487	$\cdots$	0.17	0.28	0.29
QSO 4120	0.25	0.35	0.44	0.56
Star A (3026 3408)	0.27	$\cdots$	$\cdots$	0.64
Star B (5692 4830)	0.28	$\cdots$	$\cdots$	0.63
Star C (5006 2496)	0.28	0.40	0.59	0.62
Star D (8459 6278)	0.28	0.34	$\cdots$	0.62
Star E (1231 5437)	0.29	0.36	0.58	0.63

cannot control the spectral energy distribution of the stars, we can perform repeat experiments using multiple stars from across the field.

We determined the centroid of each image and coaligned quasar and stellar PSF images to the center of the nearest pixel. We measured the Strehl ratio for each quasar and stellar PSF image, with respect to the ideal, azimuthally symmetric PSF—see Table III. We then divide the quasar Strehl ratio by each Stellar PSF Strehl ratio to produce a corrected Strehl, $S_{\text{QSO}}/S_{\text{Star}}$, after [15]. This is found to be equivalent to measuring the Strehl ratio with respect to the stellar PSF, $S_{\text{QSO-Star}}$—see Table IV—which is as expected for well-centered images. Referring to Eq. (13), we get

$$S_{\text{Star}} = \exp[-\sigma_I^2], \qquad (17)$$

so

$$S_{\text{QSO}}/S_{\text{Star}} = S_M \exp[-\sigma_\phi^2] = S_M S_\phi. \qquad (18)$$

We find that the stars produce quite stable Strehl ratios in each filter, across the field (varying at the $\lesssim 5\%$ level), while the quasars are found to vary in Strehl ratio considerably in a given filter. We measured all Strehl ratios using a range of photometric radii, from just θ_{Airy}, up to $0'.5$, and found results to be consistent within the errors at each photometric radius. We adopt $0'.25$ as our photometric radius. Errors are dominated by systematics, estimated conservatively at $\sim \pm 10\%$ as may be inferred from Fig. 5 where a few points have $S_{\text{QSO}}/S_{\text{Star}}$ ratios ~ 1.1.

TABLE IV. Strehl ratios for the UDF quasars (identifiers from [45]) with respect to stellar PSF's, $S_{\text{QSO-Star}}$, using a photometric aperture of $0.25'$.

Source	F435W	F606W	F775W	F850LP
9397	1.10 ± 0.1	1.02 ± 0.1	1.02 ± 0.1	0.98 ± 0.1
6732	0.88 ± 0.1	0.94 ± 0.1	0.95 ± 0.1	0.86 ± 0.1
9487	0.00 ± 0.5	0.42 ± 0.1	0.48 ± 0.1	0.47 ± 0.1
4120	0.90 ± 0.1	0.88 ± 0.1	0.75 ± 0.1	0.92 ± 0.1

Repeat measurements at differing photometric radii gave far lower variation $\sim 1\%$.

The Strehl ratios of each quasar from the UDF with respect to the UDF stellar PSF's are plotted in Fig. 5, against the theoretical Strehl ratio obtained for various values of α and N. Any measured degradation above the 1:1 line (shaded region) rules out that spacetime foam model, since the quasars are not sufficiently blurry. That is, the image is degraded *less* than predicted by the theoretical model. Points below the 1:1 line may indicate structure in the sources, i.e., the blurriness is above what we would expect for a given spacetime foam model and, thus, does not test the theory.

Some blurring is seen, consistent with the level expected if $\alpha = 0.655$. All models with $\alpha \leq 0.65$ are excluded by the UDF observations.

It is straight-forward to disprove a given model, by finding an unblurred quasar just a little more distant or at shorter wavelengths (higher in the plot). Points lower in the plot may imply structure in the source. However, with the data we currently have, the alternate explanation, namely, the combination of limited Strehl ratio and the signal to noise of the UDF quasar observations, is equally plausible. We are clearly not yet probing the $\alpha = 2/3$ scenario. Larger statistical samples eventually may allow us to disentangle blurring due to structure from that due to the effects of spacetime foam.

VII. DISCUSSION AND CONCLUSION

Using the UDF data, we see evidence for an increased blurring (decreased optically corrected Strehl ratio) with increasing $I(z, \alpha)/\lambda_o$. This is likely due to masking or source structure in the majority of cases, but we note that the blurring is at a level consistent with a spacetime foam model with $\alpha = 0.655$. All models with $\alpha < 0.65$ are excluded by the UDF observations.

We are not yet probing the $\alpha = 2/3$ regime, however; the UDF data are nonoptimal for this purpose as they are not at a wavelength short enough to exclude the holographic model. Indeed, we see obvious blurring in the quasar images, in some cases due either to structure or masking. Nevertheless, the UDF observations provide the strongest constraints that currently exist on spacetime foam.

We have shown that the current HST archive does not contain observations that can more tightly constrain spacetime foam models. To do this, we would need observations in the ultraviolet. While one such observation currently exists, it was made by the STIS instrument, which has a triangular PSF with no Airy ring, making the analysis we detail in Sec. VI impossible. The measurement can be done either by the new Wide Field Camera 3 instrument, which can access the very edge of the $\alpha = 2/3$-sensitive region of the parameter space at the blue end of its spectral range (using the F225W, F275W or F300X filters), or alternately
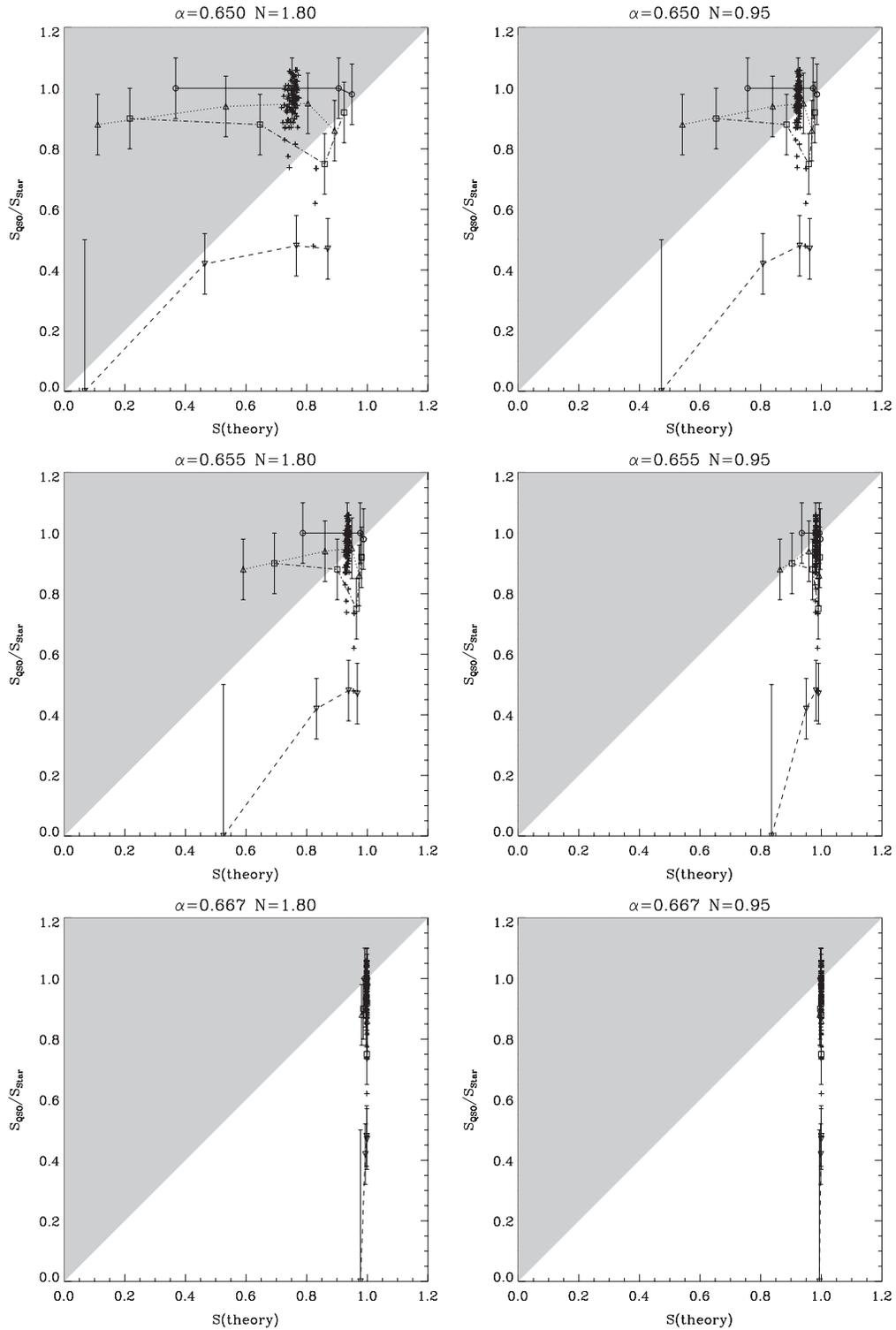
FIG. 5. Measured Strehl ratio S for the four UDF quasars (9397: circles and solid line; 6732: up-pointing triangles and dotted line; 9487: squares and dot-dashed line; 4120: down-pointing triangles and dashed line) against theoretical Strehl ratio S_ϕ (Eq. (16)), for various spacetime foam models. The shaded area indicates $S > S_\phi$: Such observations exclude a given spacetime foam model, (α, N). Crosses indicate data points from [15]. We exclude all models with $\alpha < 0.65$ since we clearly see quasars that are less blurred than is predicted by such models (top). We do in fact see a small amount of blurring in our UDF quasars, consistent with the magnitude of blurring expected for $\alpha = 0.655$ (middle). No degradation should be seen for $\alpha = 2/3$ (bottom) for the wavelengths and distances probed so far by the HST archive ($\lambda > 400$ nm).

by the ACS Solar Blind Channel, which can probe to 100 nm. While both instruments under-sample the PSF in the ultraviolet, each has its advantages. The Wide Field Camera 3 is considerably more sensitive, so that higher dynamic ranges can be probed in a shorter exposure time. However, at the short wavelengths probed by the SBC the anticipated blurring is so strong that the under-sampling may not matter.

The two main difficulties in probing high-redshift quasars at such short wavelengths are scattering by their extended haloes, and absorption by intervening HI and HeII. The former is the most likely explanation for any observed structure in the quasars, should it be observed, but can be distinguished from the effects of spacetime foam using polarimetric measurements (e.g., [48,49]). Furthermore, we do not expect scattering to dominate the flux for type 1 quasars, even at wavelengths ~ 1215 Å, since [48] found a wavelength independent scattering law for obscured quasars. The latter is the more significant problem, as we are already photon starved at rest-frame wavelengths shortward of Ly alpha, and at redshifts $\gtrsim 4.3$ both HI and HeII absorption will affect the opacity at wavelengths <1215 Å in the quasar frame [50,51]. Nevertheless, in the absence of diffraction-limited x-ray imaging in the foreseeable future, rest-frame far-UV imaging represents the best hope for probing the $\alpha = 2/3$ regime, although we admit we would be lucky to find a quasar sightline that unambiguously disproved the $\alpha = 2/3$ case by detecting no blurring or structure. In the rather more likely event of structure being detected, it would take a series of deep and expensive observations to establish that the blurring or structure was not due to scattering. The best sources to investigate are the high resdshift quasars from the Richards (SDSS) catalog that are known to be isolated and to show no structure in their z or I band images. All the UDF quasars show companions or similar nearby structure.

As already noted at the end of Sec. V, one of the most exciting prospects is that the fully operational VLTI will allow us to test the holographic model. In fact, as shown by Fig. 1, due to the combination of its baseline size plus wavelength, the VLTI emerges as the best overall current or planned instrument for the testing of spacetime foam models. The instrumental setup to use would be either the Mid-infrared Interferometric Instrument (at wavelengths longer than 5 μm) or phase referenced imaging and micro-arcsecond astrometry (at shorter wavelengths). This would be a rather difficult observation, because currently, VLT interferometry is limited to the very brightest sources: in K band, the practical limit is $K = 10$, although that can be extended down to $K = 15$ if a bright star of $K = 10$ or brighter is very close to (within a few arcseconds) the quasar (F. Delplancke, priv. comm.). The presence of such a bright point source allows one to ''phase-reference'' the observation so that the visibility

of the fringes can be tracked with high precision. This is a significant difficulty, as the number of quasars brighter than $K = 10$ is very small—in fact, a search in Set of Identifications, Measurements, and Bibliography for Astronomical Data revealed only one such object, namely, 3C 273, which is at the modest redshift of $z = 0.158$. If one looks for bright stars within 40 arc sec, one finds a few other quasars with bright stars nearby, specifically PKS 0435-300, HS 1227+464', OK 568, AH 26 and 2GZ J011339-3343. All of these are at the lower end of the useful range as far as the quasar brightness is concerned, and also, two or three are too far north for VLTI observations (HS 1227_4641, OK 568, possibly AH 26).

The initial conclusion would then be that this is a difficult observation to do and not many sources are available to do it. However, one can use targets of opportunity to explore further. For example, bright blazars in outburst can reach up to $K \sim 12$ and in extreme cases $K \sim 11$, making them possibly useful for these observations, particularly if the future holds an increase in sensitivity. Another possibility is to use the afterglows of bright gamma-ray bursts, which have now in at least one case gotten considerably brighter than 10th magnitude in K. Examples here include GRB 990123, which reached $V \sim 9$ in its prompt phase (Galama *et al.* 1999), and GRB 060607A (Ziaeepour *et al.* 2008), which was $B \sim 13$ in its prompt phase. However, considering that GRBs decline precipitously in brightness within minutes, their utility for VLTI observations is likely quite limited.

We conclude with a succinct summary. In this paper we elaborate on an earlier proposal (CNvD, 2006) to detect spacetime foam by looking for seeing disks in the images of distant quasars and AGNs. Assuming isotropic fluctuations, we argue that spacetime in effect creates a seeing disk whose angular diameter is $\sim \delta \psi$ and that the effect is expected to show up in interferometric fringe pattern as decreasing fringe visibility and reduction in Strehl ratios as soon as $\delta \psi \sim \lambda / D$. A model of spacetime foam is disproved if images of a distant source do not exhibit the blurring predicted by the model. Thus far, images of high-redshift quasars from HUDF provide the most stringent tests of spaceteime foam models. The random-walk model is convincingly ruled out while the holographic model is still viable. We anticipate that the latter model can be tested when the VLTI is fully operational; it is also possible that observations with HST in the ultraviolet may accomplish this goal.

Fosbury for useful comments. Y. J. N. thanks A. Glindemann for the hospitality extended to him while he was visiting the Headquarters of ESO. This paper is partly based on observations with the NASA/ESA *Hubble Space Telescope*, obtained at the Space Telescope Science Institute.

[1] J. A. Wheeler, in *Relativity, Groups and Topology*, edited by B. S. DeWitt and C. M. DeWitt (Gordon and Breach, New York, 1963), p. 315.
[2] Y. J. Ng, Mod. Phys. Lett. A **18**, 1073 (2003).
[3] R. Lieu and L. W. Hillman, Astrophys. J. **585**, L77 (2003).
[4] Y. J. Ng, W. Christiansen, and H. van Dam, Astrophys. J. **591**, L87 (2003).
[5] R. Ragazzoni, M. Turatto, and W. Gaessler, Astrophys. J. **587**, L1 (2003).
[6] W. Christiansen, Y. J. Ng, and H. van Dam, Phys. Rev. Lett. **96**, 051301 (2006).
[7] G. Amelino-Camelia, Nature (London) **398**, 216 (1999).
[8] F. Karolyhazy, Nuovo Cimento A **42**, 390 (1966).
[9] Y. J. Ng and H. van Dam, Mod. Phys. Lett. A **9**, 335 (1994).
[10] Y. J. Ng and H. van Dam, Mod. Phys. Lett. A **10**, 2801 (1995).
[11] L. Susskind, J. Math. Phys. (N.Y.) **36**, 6377 (1995).
[12] G. 'tHooft, in *Salamfestschrift*, edited by A. Ali *et al.* (World Scientific, Singapore, 1994), p. 284.
[13] C. W. Misner, K. S. Thorne, and J. A. Wheeler, *Gravitation* (Freeman, San Francisco, 1973), p. 1190.
[14] D. W. Hogg, arXiv:astro-ph/9905116.
[15] E. Steinbring, Astrophys. J. **655**, 714 (2007).
[16] A. A. Abdo *et al.*, Nature (London) **462**, 331 (2009).
[17] Y. J. Ng, Entropy **10**, 441 (2008).
[18] E. S. Perlman *et al.*, Astron. J. **124**, 2401 (2002).
[19] V. Giovannetti, S. Lloyd, and L. Maccone, Science **306**, 1330 (2004).
[20] S. Lloyd and Y. J. Ng, Sci. Am. **291**, No. 5, 52 (2004).
[21] N. Margolus and L. B. Levitin, Physica (Amsterdam) **120D**, 188 (1998).
[22] Y. J. Ng, Phys. Rev. Lett. **86**, 2946 (2001); **88**, 139902(E) (2002).
[23] Y. J. Ng and H. van Dam, Found. Phys. **30**, 795 (2000).
[24] H. Salecker and E. P. Wigner, Phys. Rev. **109**, 571 (1958).
[25] E. P. Wigner, Rev. Mod. Phys. **29**, 255 (1957).
[26] J. Ellis, N. Mavromatos, and D. V. Nanopoulos, Phys. Lett. B **293**, 37 (1992).
[27] R. Blandford and R. Narayan, Astrophys. J. **310**, 568 (1986).
[28] G. Amelino-Camelia, J. Ellis, N. E. Mavromatos, D. V. Nanopoulos, and S. Sarkar, Nature (London) **393**, 763 (1998).
[29] B. Mobasher, P. Capak, N. Z. Scoville, T. Dahlen, M. Salvato, H. Aussel, D. J. Thompson, R. Feldmann, L. Tasca, O. Lefevre, S. Lilly, C. M. Carollo, J. S. Kartaltepe, H. McCracken, J. Mould, A. Renzini, D. B. Sanders, P. L. Shopbell, Y. Taniguchi, M. Ajiki, Y. Shioya, T. Contini, M. Giavalisco, O. Ilbert, I. Iovino, V. LeBrun, V. Mainieri, M. Mignoli, and M. Scodeggio, Astrophys. J. Suppl. Ser. **172**, 117 (2007).
[30] X.-B. Wu and Z. Jia, Mon. Not. R. Astron. Soc. **406**, 1583 (2010).
[31] K. I. Kellermann *et al.*, Astrophys. J. **609**, 539 (2004).
[32] K. I. Kellermann, R. C. Vermeulen, J. A. Zensus, and M. H. Cohen, Astron. J. **115**, 1295 (1998).
[33] P. M. Ogle, M. H. Cohn, J. Miller, H. D. Tran, R. A. E. Fosbury, and R. W. Goodrich, Astrophys. J. **482**, L37 (1997).
[34] H. Wolter, Ann. Phys. (Leipzig) **445**, 94 (1952).
[35] H. Wolter, Ann. Phys. (Leipzig) **445**, 286 (1952).
[36] D. G. Sandler *et al.*, J. Opt. Soc. Am. A **11**, 925 (1994).
[37] D. P. Schneider, P. B. Hall, G. T. Richards, M. A. Strauss, D. E. V. Berk, S. F. Anderson, W. N. Brandt, X. Fan, S. Jester, J. Gray, J. E. Gunn, M. U. SubbaRao, A. R. Thakar, C. Stoughton, A. S. Szalay, B. Yanny, D. G. York, N. A. Bahcall, J. Barentine, M. R. Blanton, H. Brewington, J. Brinkmann, R. J. Brunner, F. J. Castander, I. Csabai, J. A. Frieman, M. Fukugita, M. Harvanek, D. W. Hogg, Ž. Ivezić, S. M. Kent, S. J. Kleinman, G. R. Knapp, R. G. Kron, J. Krzesiński, D. C. Long, R. H. Lupton, A. Nitta, J. R. Pier, D. H. Saxe, Y. Shen, S. A. Snedden, D. H. Weinberg, and J. Wu, Astron. J. **134**, 102 (2007).
[38] G. T. Richards, M. A. Strauss, B. Pindor, Z. Haiman, X. Fan, D. Eisenstein, D. P. Schneider, N. A. Bahcall, J. Brinkmann, and R. Brunner, Astron. J. **127**, 1305 (2004).
[39] M.-P. Veron-Cetty and P. Veron, Astron. Astrophys. **518**, A10 (2010).
[40] G. T. Richards, Z. Haiman, B. Pindor, M. A. Strauss, X. Fan, D. Eisenstein, D. P. Schneider, N. A. Bahcall, J. Brinkmann, and M. Fukugita, Astron. J. **131**, 49 (2006).
[41] R. L. White, R. H. Becker, X. Fan, and M. A. Strauss, Astron. J. **129**, 2102 (2005).
[42] M. Stiavelli, in HST Proposal, p. 9777+ (2003).
[43] M. J. Kukula, J. S. Dunlop, R. J. McLure, L. Miller, W. J. Percival, S. A. Baum, and C. P. O'Dea, Mon. Not. R. Astron. Soc. **326**, 1533 (2001).
[44] S. Savaglio, Astron. J. **116**, 1055 (1998).
[45] C. Xu, N. Pirzkal, S. Malhotra, J. E. Rhoads, B. Mobasher, E. Daddi, C. Gronwall, N. P. Hathi, N. Panagia, H. C. Ferguson, A. M. Koekemoer, M. Kümmel, L. A. Moustakas, A. Pasquali, S. di Serego Alighieri, J. Vernet, J. R. Walsh, R. Windhorst, and H. Yan, Astron. J. **134**, 169 (2007).
[46] S. V. W. Beckwith, M. Stiavelli, A. M. Koekemoer, J. A. R. Caldwell, H. C. Ferguson, R. Hook, R. A. Lucas, L. E. Bergeron, M. Corbin, S. Jogee, N. Panagia, M. Robberto, P. Royle, R. S. Somerville, and M. Sosey, Astron. J. **132**, 1729 (2006).

[47] N. Pirzkal, C. Xu, S. Malhotra, J. E. Rhoads, A. M. Koekemoer, L. A. Moustakas, J. R. Walsh, R. A. Windhorst, E. Daddi, A. Cimatti, H. C. Ferguson, J. P. Gardner, C. Gronwall, Z. Haiman, M. Kümmel, N. Panagia, A. Pasquali, M. Stiavelli, S. di Serego Alighieri, Z. Tsvetanov, J. Vernet, and H. Yan, Astrophys. J. Suppl. Ser. **154**, 501 (2004).

[48] J. Vernet, R. A. E. Fosbury, M. Villar-Martín, M. H. Cohen, A. Cimatti, S. di Serego Alighieri, and R. W. Goodrich, Astron. Astrophys. **366**, 7 (2001).

[49] S. Young, D. J. Axon, A. Robinson, and A. Capetti, Astrophys. J. **698**, L121 (2009).

[50] P. Madau, Astrophys. J. **441**, 18 (1995).

[51] A. Meiksin, Mon. Not. R. Astron. Soc. **365**, 807 (2006).